Rare Metal Materials and Engineering
Volume 50, Issue 7, July 2021
Available online at www.rmme.ac.cn

Science Press

Cite this article as: Zong Xuewen, Wang Lei, Liu Wenjie, et al. Effect of Withdrawal Rate of Spiral Selector on Grain Selection Behavior and Grain Orientation Evolution[J]. Rare Metal Materials and Engineering, 2021, 50(07): 2366-2374.

ARTICLE

Effect of Withdrawal Rate of Spiral Selector on Grain Selection Behavior and Grain Orientation Evolution

Zong Xuewen[1], Wang Lei[1], Liu Wenjie[1], Zhang Bin[1], Zhang Lingfeng[2]

[1] College of Mechanical Engineering, Xi'an University of Science and Technology, Xi'an 710054, China; [2] Xi'an Hangfa Precision Casting Co., Ltd, Xi'an 710021, China

Abstract: The grain selection process during single-crystal casting of a Ni-base superalloy DD5 in a spiral grain selector was simulated by a macroscale ProCAST coupled with a mesoscale cellular automaton finite element (CAFE) model, and the simulation results were validated by experimental observations. The results show that at the same withdrawal rate, the number of dendrites decreases gradually, and the primary dendrite arm spacing increases gradually with the increase of the distance from the chill surface. With increasing the withdrawal rate from 2 mm/min to 8 mm/min, the primary dendrite arm spacing decreases, the number of dendrite stems increases, the dendrite spacing decreases and the dendrite structure is refined gradually. During the simulation process, the quantity, area, and color of the solid tissue are similar at the three withdrawal rates of the spiral selector starter block. In the spiral part, the microstructures at 5 mm/min are less than those at the other two withdrawal rates, with larger area and lighter color. The grain selection efficiency at the intermediate withdrawal rate is better than that at the other two withdrawal rates, which is obtained from the results of the grain microstructure evolution and metallographic microstructure analysis of crystal selector.

Key words: spiral selector; grain selection behavior; withdrawal rate; directional solidification; primary dendrite arm spacing

Ni-based single-crystal superalloy is widely used in aeroengine and industrial gas turbine blades for its excellent high-temperature strength and creeps resistance[1-3]. Compared with the traditional casting blades, the single-crystal turbine blades have higher service temperatures and better mechanical properties due to the elimination of grain boundaries[4]. The blade with single-crystal structure obtained by directional solidification is achieved by a crystal selector. And the structure of the crystal selector directly affects the efficiency of grain selection, product qualification, and yield. The types of crystal selector mainly include necking, turning, inclined, and spiral types, and the difference between the four types of crystal selector is mainly due to different spiral parts. At present, the spiral selector has been widely used with good grain selection efficiency, but its optimal parameters and spatial structure are complex and difficult to obtain, which has attracted increasing attentions from scholars[5-7].

The key components of a spiral selector include the starter block and the spiral part[8], as shown in Fig. 1. The starter block mainly completes the grain chilling nucleation and competitive growth, and the grains with larger orientation deviation from the heat flow direction are eliminated to ensure that a certain number of grains with smaller orientation deviation angle enter the spiral part. The main function of the spiral part is to remove most of the grains according to the geometric constraints, and finally to select a grain with the minimum deflection angle with the <001> orientation[9]. Researches on crystal selection and selector structure designs have been conducted by scholars through analytical, experimental, and simulation methods. D'Souza et al[10] studied the effect on the grain growth direction of isothermal surfaces along different directions. The effect of initial grain position distribution and the secondary dendrite arm orientation on the grain growth in the starter block and spiral part was studied by Zhang et al[11]. Liu et al[12] expounded the principle of dendrite growth in a spiral selector by studying the dendrite arm spacing. The principle of grain selection for different crystal selectors was revealed by Zheng et al[13]. Jiang et al[14]

Received date: July 12, 2020
Foundation item: National Natural Science Foundation of China (51875452)
Corresponding author: Zong Xuewen, Ph. D., Associate Professor, College of Mechanical Engineering, Xi'an University of Science and Technology, Xi'an 710054, P. R. China, E-mail: zongw007@xust.edu.cn

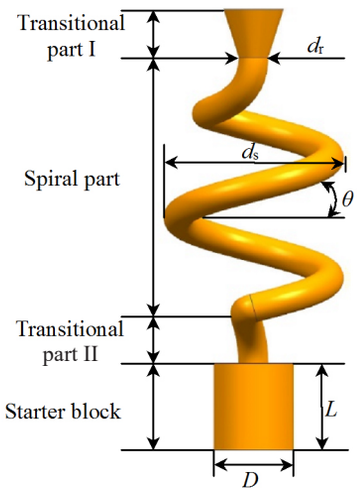

Fig.1 Schematic diagram of spiral selector[8]

effectively analyzed the influence of grain orientation and grain phase on the seeding process by studying the grain selection process of Ni_3Al-based superalloy. Yan et al[15] studied the relationship among temperature, grain microstructure, and grain growth. As for the selector structure design, Esaka et al[16] revealed that the evolutions of grain structures and crystal orientations during single-crystal casting significantly depend on the geometries of the starter block (length L and width D). Dai et al[17] simulated and analyzed the competitive growth and grain selection in the selector with emphasis on the geometric parameters of spiral (spiral angle θ, spiral thickness d_s, and spiral rotation diameter d_r), using a ProCAST coupled with a mesoscale cellular automaton finite element (CAFE) model. Zhang et al[18] studied the effect of a spiral angle on the crystal selector, and the results show that the crystal selector with a smaller spiral angle effectively reduces the deviation of preferred orientation. The grain selection behavior of the spiral selector has attracted much attention from scholars. However, there are few studies about the effect of process parameters on the grain selection behavior of the spiral selector during the grain selection process.

To improve the production efficiency and yield rate of single-crystal blades, it is imperative to investigate the influence of process parameters on the selection behavior of the crystal selector. Among the process parameters, the withdrawal rate is easy to adjust for producing single-crystal blades under different conditions. During the process of directional solidification, it is beneficial to improve the withdrawal rate for better production efficiency, and the primary dendrite arm spacing (PDAS, λ) reduces[19], resulting in the decrease of microsegregation[20], the reduction of subsequent heat treatment time, and the improvement of mechanical properties. Unfortunately, as the withdrawal rate increases, the frequency of stray grain formation increases[21]. An optimum withdrawal rate is therefore a key to fabricate single-crystal turbine blades.

The influence of the withdrawal rate on the grain selection behavior of the spiral selector was studied by the method of experimental investigations and finite element simulations in this research. The investigation was focused on the grain selection efficiency of the spiral selector at different withdrawal rates. And the influence of the withdrawal rate of a spiral selector on the grain microstructure growth was revealed at microscopic scale, and then the withdrawal rate of the spiral selector with higher grain selection efficiency was selected. These results were expected to improve the grain selection efficiency of the spiral selector. The structural parameters of the spiral selector used in this study were selected from the conventional industrial parameters. The specific parameters are shown in Table 1.

1 Experiment and Simulation Methods

1.1 Experiment

The material used in this study was the second-generation single-crystal superalloy DD5, whose nominal chemical composition is presented in Table 2. The refractory alumina and copper were used for the shell and water-cooled copper platform, respectively.

The directional solidification experiment of a single-crystal blade was conducted in a Bridgman directional solidification furnace. The directional solidification furnace was simplified into three parts: heating zone, fixed baffler, and cooling zone, as shown in Fig. 2. In each experiment, a wax mold of the crystal selector was used to prepare the shell mold, and the process of the directional solidification was as follows: heating-melting-pouring-standing-withdrawal-cooling.

Table 1 Structure parameters of spiral selector

d_r/mm	d_s/mm	L/mm	D/mm	θ/(°)
8	30	17	16	20

Table 2 Chemical composition of DD5 superalloy (wt%)

Cr	Co	Mo	W	Al	Ta	C	B	Hf	Ni
7.0	7.5	1.5	5.0	6.2	6.5	0.05	0.04	0.15	Bal.

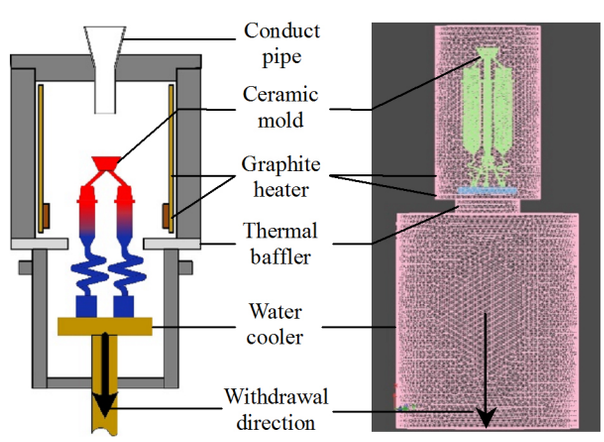

Fig.2 Schematic diagram and finite element method mesh model of furnace chamber and casting system

Before pouring, the mold was installed on the water-cooled copper cooling plate, and the furnace chamber emptied to a partial pressure of ~100 Pa. The pouring temperature was 1500 °C, and the cooling water temperature was 40 °C. The DD5 nickel superalloy was poured into the mold at the same temperature and held for 2 min to stabilize the melt[22]. Finally, the ceramic mold was pulled out from the furnace at different withdrawal rates of 2, 5, and 8 mm/min, i. e., small, intermediate, and large withdrawal rates, respectively.

After the casting process, the remnant mold was removed from the crystal selector surface with sandpaper. Then the crystal selector was sectioned from the sample transversely (parallel to the *XY* plane), and the cross sections S1~S6 were obtained and prepared for metallographic analysis. After standard metallographic techniques were employed for the preparation of specimens, polished surfaces were etched to reveal the dendrite structure using a solution containing 10 mL HCl, 4 mL HF, and 30 mL H_2O_2. Dendrite morphologies of samples were observed by optical microscope (OM)[23,24].

As an important microstructural scale in directional solidification, the PDAS, as shown in Fig. 3, has a significant effect on the mechanical properties of subsequent casting products in the directional solidification of superalloys. Therefore, it is necessary to study the primary dendrite arm spacing during the grain selection process. After the metallographic preparation, the PDAS was calculated by the area counting method on the transverse sections by Eq.(1), as follows[25]:

$$\lambda = c\sqrt{A/N} \tag{1}$$

where A is the area of the section of specimen; N is the number of dendrites in this area; c is a constant equaling 1[26].

1.2 Simulation process

1.2.1 Directional solidification process

During the directional solidification process, after simplifying the simulation conditions, the physical model includes directional solidification furnace and single-crystal casting. As shown in Fig. 2, the directional solidification furnace includes heating zone, fixed baffler, and cooling zone. The directional solidification furnace and casting were modeled by the 3D modeling software UG, and the directional solidification process of single-crystal casting was simulated by the finite element analysis software ProCAST. The gating system for casting single-crystal blade mainly includes the gate, blade, crystal concentrator, impurity filter, and water-cooled copper disk.

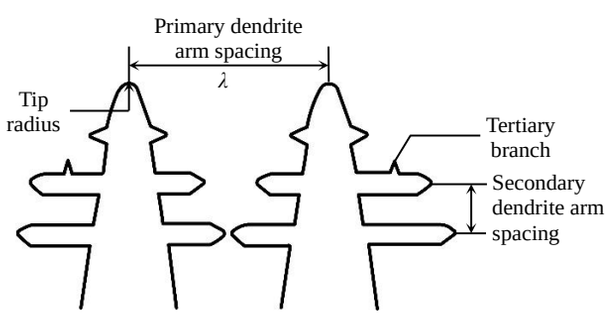

Fig.3 Schematic diagram of different length scales

In the preprocessing module of ProCAST software, the physical models of single-crystal casting meshed. Fig. 2 illustrates the finite element method (FEM) mesh model of the casting system corresponding to the Bridgman furnace. Because the furnace body only radiates heat, the directional solidification equipment was divided into two-dimensional grids. To reduce the calculation time, the grid size was 10 mm, and there were many design process parameters of the gating system of single-crystal casting. Therefore, a three-dimensional grid was divided. However, due to different structural dimensions of each region of the gating system, the gating system was divided into different regions. The largest part of the grid was 3 mm, and the smallest part was 1 mm. To better meet the actual process conditions, the single-crystal casting was investment cast. After the casting mesh was divided, the mold shell was generated, and the uniform mold shell with a thickness of 6 mm was automatically generated by the investment casting module of ProCAST. In the present model, the relative motion between the mold and the furnace was achieved through the upward movement of enclosure, and the withdrawal rate was set as 2, 5, and 8 mm/min.

1.2.2 Process parameters and boundary condition

During the directional solidification, the temperatures of heating zone, heat insulation baffle, cooling zone, and water-cooled copper platform of the spiral selector system were 1470, 960, 20, and 25 °C, respectively. The interface heat transfer of directional solidification of singlecrystal casting consists of three parts: (1) interface heat transfer among the singlecrystal blade, and spiral selector directional solidification shell, and casting, h_1=100 $W\cdot m^{-2}\cdot °C^{-1}$; (2) interface heat transfer among the singlecrystal blade, spiral selector directional solidification shell, water-cooled copper platform, h_2=100 $W\cdot m^{-2}\cdot °C^{-1}$; (3) interface heat transfer among the singlecrystal blade, spiral concentrator directional solidification casting, and water-cooled copper platform, h_3=5000 $W\cdot m^{-2}\cdot °C^{-1}$.

1.2.3 Nucleation model

In the simulation of spiral crystal selector with CAFE model in ProCAST, the nucleation density and the dendrite tip growth kinetics of DD5 nickel-based single-crystal superalloy solution were calculated by Gauss distribution and Kurz-Giovanola-Trivedi (KGT) model[27], respectively. Therefore, the Gauss distribution model was used to calculate the nucleation densities in undercooled metals at the nucleation initiation surface of helical crystal selector and the front solidification interface of DD5nickel-based single-crystal superalloy solution. The continuous nucleation distribution, dn/d(ΔT), can be described by Eq.(2) as follows[28]:

$$\frac{\mathrm{d}n}{\mathrm{d}(\Delta T)} = \frac{n_{\max}}{\sqrt{2\pi\Delta T_\sigma}} \exp\left(-\frac{\Delta T - \Delta T_{\max}}{2\Delta T_\sigma}\right) \tag{2}$$

where n is the nucleation density of DD5 nickel-based single-crystal superalloy solution; dn is the grain density increment,

which is induced by an increment of the undercooling d(ΔT); ΔT_{max} is the mean undercooling; ΔT_{σ} is the standard deviation; n_{max} is the maximum density of nuclei obtained by the integral of the Gaussian distribution.

1.2.4 Grain growth model

During the practical production, the contact surface between the starter block of the spiral selector and the chill plate surface is a circular nucleation surface, and the direction of the withdrawal rate is Z direction, which results in the crystal orientation of the spiral selector with <001> positive random distribution. The <001> oriented grains can meet the complex stress-strain requirements of blades. To explain the growth model of dendrite at the tip front in the spiral selector, the ProCAST software adopted "cell capture" method to simulate the growth of dendrite at the tip front of solid-liquid phase, and then calculated the growth model of dendrite at the tip front of solid-liquid phase in spiral selector through KGT model. The growth rate polynomial of the dendrite tip of DD5 single-crystal superalloy solution obtained by calculation is expressed by Eq.(3) as follows[29]:

$$v = a_2\Delta T^2 + a_3\Delta T^3 \quad (3)$$

where a_2 and a_3 are coefficients of higher-order polynomials determined by alloy composition according to the KGT model; ΔT is the undercooling of the growth front of dendrite tip of DD5 single-crystal superalloy solution; v is the growth rate of dendrite tip in DD5 single-crystal superalloy solution. The undercooling of DD5 single-crystal superalloy solution at the growth front of dendrite tip during directional solidification of the single-crystal blade is mainly composed of four parts, which is expressed by Eq. (4) as follows:

$$\Delta T = \Delta T_C + \Delta T_T + \Delta T_K + \Delta T_R \quad (4)$$

where ΔT_C is the composition undercooling of DD5 single-crystal superalloy solution, ΔT_T is the thermodynamic undercooling of DD5 single-crystal superalloy, ΔT_K is the growth kinetics undercooling of DD5 single-crystal superalloy, and ΔT_R is the undercooling degree of solid-liquid interface curvature of DD5 single-crystal superalloy solution.

1.2.5 Competitive growth of grains

The grain selection process of crystal selector was simulated by the ProCAST coupled with CAFE model in this work. In the CAFE model, the grain orientation at the bottom of the starter block is random. When the grain grows to a certain height, the <001> orientation (preferred growth direction) of most of the grains is parallel or close to the Z direction (stress axis direction). According to Eq.(3), the growth rate of grain tip depends on the temperature gradient in front of the dendrite tip. Therefore, the smaller the angle θ between the direction of the grain growth rate and the direction of the maximum gradient of the temperature field, the larger the grain growth rate. This phenomenon made the grains with smaller angles grow the secondary and tertiary side arms and occupy the space just in front of the grains with larger angles, as shown in Fig.4, referring as the grain competitive growth.

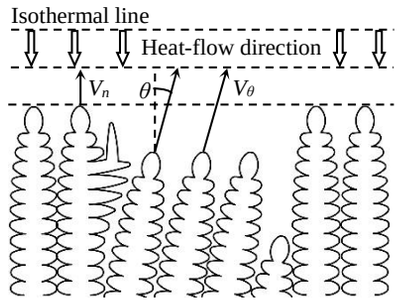

V_n-positive dendrites growth rate, V_θ-oblique dendrites growth rate

Fig.4 Schematic diagram of grain competitive growth[30]

2 Results and Discussion

2.1 Evolution of metallographic microstructure in crystal selector with different withdrawal rates

The macroscopic morphologies of the spiral selector at withdrawal rates of 2, 5, and 8 mm/min are shown in Fig.5a~5c, respectively. The spiral selector consists of a starter block and a spiral part, as shown in Fig. 1. Three spiral selectors were sliced perpendicularly to the <001> orientation, as indicated by S1~S6 in Fig.5, and the dendrite morphologies of samples were observed by OM.

Before the solidification of single-crystal blade gets into the steady-state growth, a non-steady-state microstructure evolution process occurs in the crystal selector starter block. During the process of grain selection, the starter block plays an important role. When the alloy nucleates rapidly through the chilled plate, a large number of grains with different orientations form. As the shell moves slowly, the solid-liquid interface pushes forward along the opposite direction of the heat flow. The intergranular growth is competitive. During the solidification process, the grains with a large deviation angle from <001> grain orientation are gradually eliminated.

The OM images of the cross sections S1, S2, and S3 of starter block of the spiral selector at different withdrawal rates are shown in Fig.6. At the initial position of the starter block (S1), the number of dendrites in the sections at different withdrawal rates is large, the dendrite spacing is small, and all

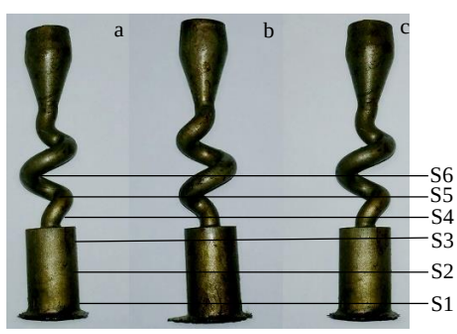

Fig.5 Appearance of spiral selector with different withdraw rates: (a) 2 mm/min, (b) 5 mm/min, and (c) 8 mm/min

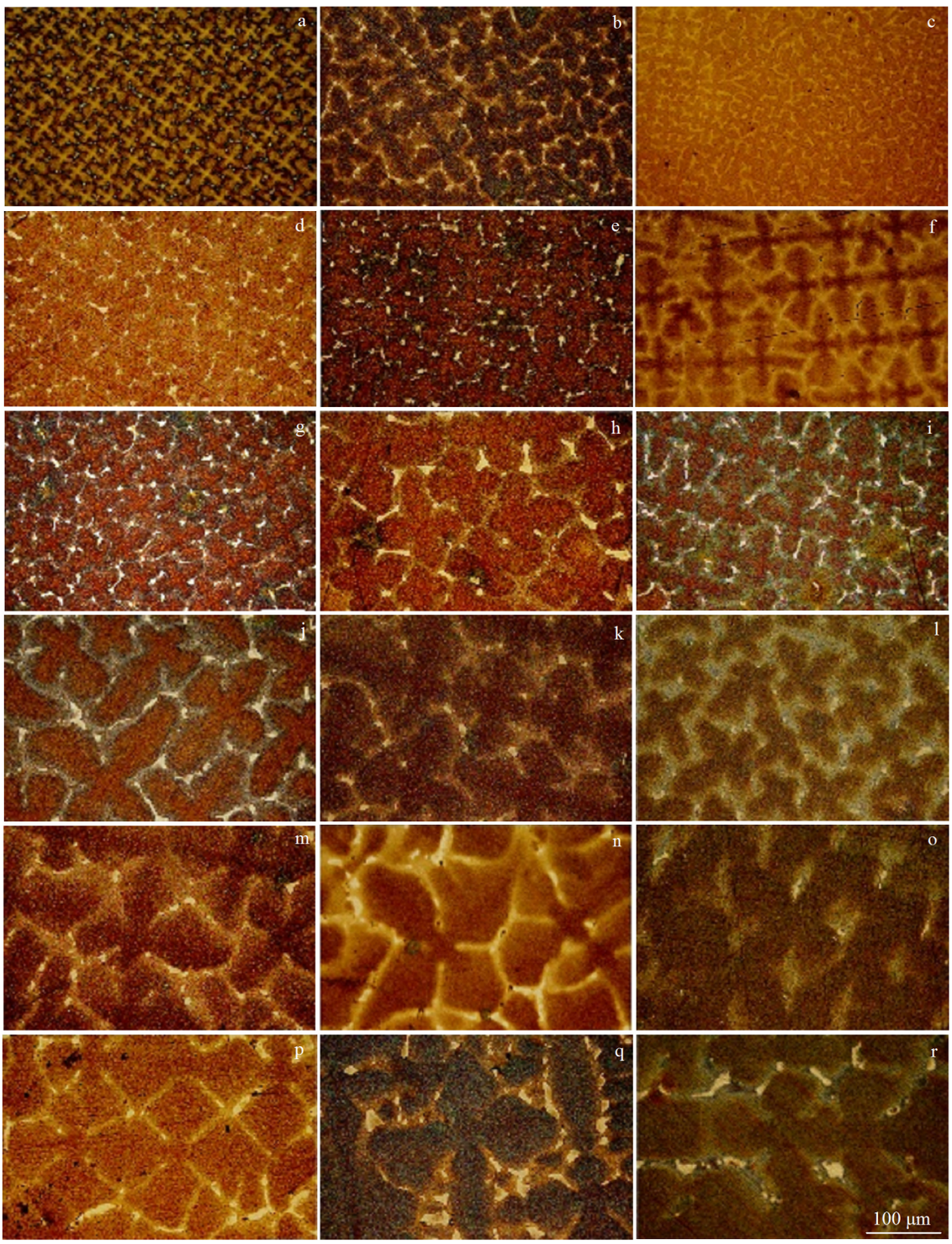

Fig.6 OM images of cross sections S1 (a~c), S2 (d~f), S3 (g~i), S4 (j~l), S5 (m~o), and S6 (p~r) of spiral selector at different withdraw rates: 2 mm/min (a, d, g, j, m, p) , 5 mm/min (b, e, h, k, n, q) , and 8 mm/min (c, f, i, l, o, r)

the dendrites are densely arranged, as shown in Fig. 6a~6c, showing that the chilled surface produces a large number of dendrites with tiny structure and different directions, and the increase of dendrites is helpful for the crystal selector to select dendrites. When the dendrites reach the intermediate position (S2), the number of dendrites in the sections at different withdrawal rates significantly reduces, the dendrite spacing increases, and the hypertrophy phenomenon at partial dendrite end occurs, as shown in Fig. 6d~6f, indicating the numerous dendrites with a larger angle between <001> orientation and dendrites die when the dendrites pass through the initial selection of the induction section, which provides the growth

energy and space for other dendrites. At the end of the starter block (S3), the number of dendrites in the sections at different withdrawal rates significantly reduces, the grain spacing is basically the same, no phenomenon of dendrite end coarsening and larger individual dendrites occurs, and there are obvious blank areas between dendrites, as shown in Fig.6g~6i, indicating the dendrites with a larger angle between <001> orientation and dendrites die, and the remaining dendrites get enough growth space.

With the increase of distance from the chill surface, the number of dendrites decreases gradually, and the primary dendrite arm spacing increases gradually. The smaller the number of dendrites, the larger the space of dendrite growth, the larger the dendrite spacing, and the faster the single-crystal selection rate. Therefore, it can be intuitively found that the number of dendrites in the same cross section at the intermediate withdrawal rate is less than that at the other two withdrawal rates. So, the selection efficiency at the intermediate withdrawal rate is better than that at the other two withdrawal rates.

The primary arm dendrite spacing in each section of the starter block of the spiral selector at different withdrawal rates is shown in Table 3. With the increase of withdrawal rate, the primary dendrite arm spacing decreases, the number of dendrite stems increases, the dendrite spacing decreases, and the dendrite structure is refined gradually.

The grains in the starter block of the spiral selector suffer competitive growth, and the grains with a large difference in orientation are eliminated. The remaining grains enter the spiral part of the crystal selector. The main function of the spiral part is to provide special structural constraints for grain growth, and only one kind of grains completes the competitive growth. The process of grain selection fails when the grains competing for growth at the same time are generated with multiple orientations in the blade.

The OM images of the cross sections S4, S5, and S6 of the spiral part of the spiral selector at different withdrawal rates are also shown in Fig.6. The grains after screening by the starter block enter the spiral part. At the initial position of the spiral part (S4), the dendrites in section at different withdrawal rates sharply reduce, the primary arm spacing significantly increases, and obvious grain boundaries appear, as shown in Fig.6j~6l, showing that the structure restriction of the spiral part plays an important role in the dendrite growth. When the dendrites reach the middle of the spiral part (S5), the number of dendrites in section at different withdrawal rates significantly reduces, the dendrite spacing increases, and the hypertrophy phenomenon of local dendrite end occurs, as shown in Fig.6m~6o, indicating that due to the restriction of the spatial structure of the spiral part, the dendrites with a large difference in the growth direction and spiral part structure vanish after the competition, which provides the growth energy and space for other dendrites. At the end of the spiral part (S6), the number of dendrites in section at different withdrawal rates significantly reduces, and a single-crystal structure of dendrites initially forms, as shown in Fig.6p~6r.

Under the condition of the same withdrawal rate, with the increase of the distance from the chill surface, the number of dendrites decreases, and the primary dendrite arm spacing increases gradually. It can be intuitively found that the number of dendrites in the same cross section at the intermediate withdrawal rate is less than that at the other two withdrawal rates. Also, the crystal selector at the intermediate withdrawal rate is the first to select the single crystal, so the grain selection efficiency at the intermediate withdrawal rate is better than that at the other two withdrawal rates.

The primary arm dendrite spacing in each section of the spiral part of the spiral selector at different withdrawal rates is also shown in Table 3. It can be found that with the increase of withdrawal rate, the primary dendrite arm spacing decreases, the number of dendrite stems increases, the dendrite spacing decreases, and the dendrite structure is refined gradually.

The relationship between primary dendrite arm spacing and chill surface distance is shown in Fig. 7, indicating that the changing trends of the primary dendrite arm spacing of crystal selector at different withdrawal rates are similar. But there is still a significant difference in the specific change process of the primary dendrite arm spacing. At the same withdrawal rate, the primary dendrite arm spacing increases with the distance from the chilled surface. With increasing the withdrawal rate, the primary dendrite arm spacing gradually

Table 3 Primary arm dendrite spacing (λ) at different withdrawal rates in starter block and spiral part of spiral selector (μm)

Cross section	Withdrawal rate/mm·min^{-1}		
	2	5	8
S1	118	78	66
S2	141	132	106
S3	198	157	148
S4	264	216	195
S5	374	289	244
S6	648	374	355

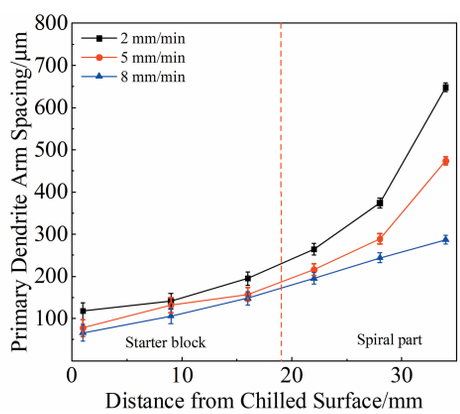

Fig.7 Relationship between primary dendrite arm spacing and distance from chilled surface

decreases in the same chilled surface. Also, when the distance between the crystal selector and chilled surface is within 8 mm, the primary dendrite arm spacing significantly increases. When the distance between the crystal selector and chilled surface is 8~17 mm, the increase rate of primary dendrite arm spacing slows down. Similarly, the primary dendrite arm spacing significantly increases with the distance between the spiral selector and the chilled surface above 18 mm. According to the final result, in the same chilled surface, the crystal selector at the intermediate withdrawal rate selects the single crystal firstly, indicating that the grain selection efficiency at the intermediate withdrawal rate is better than that at the other two withdrawal rates.

2.2 Grain microstructure evolution in crystal selector with different withdrawal rates

The numerical simulation of the microstructure growth of crystal in the spiral crystallizer was conducted by ProCAST software with CAFE model, and the simulation results of the grain structure evolution of the spiral crystallizer under different withdrawal rates are obtained. Fig. 8a~8c are the simulation results of grain microstructure evolution of spiral selector at the withdrawal rate of 2, 5, and 8 mm/min, respectively. And orientation images and corresponding <001> pole figures in different sections can be obtained through the cross sections S1~S6 in Fig.8.

The orientation image maps and corresponding <001> pole figures of three cross sections (S1~S3) of the starter block in the spiral selector at withdrawal rates of 2, 5, and 8 mm/min are obtained. Different colors represent different angles between different growth directions of grains, and different shapes represent different spatial structures of grains, as shown in Fig.9.

The solidified microstructure at the bottom of the chilled surface in contact with the chill-plate consists of tiny and randomly oriented grains (huge color difference). The larger the distance from the chilled surface, the larger the solidification microstructure and the lighter the color, which indicates that the angle between grain growth direction and <001> orientation is small. Due to the cooling effect of the chill plate on the singlecrystal superalloy solution, a large number of crystal nuclei with random orientation form on the surface of the chill-plate at the bottom of the starter block of crystal

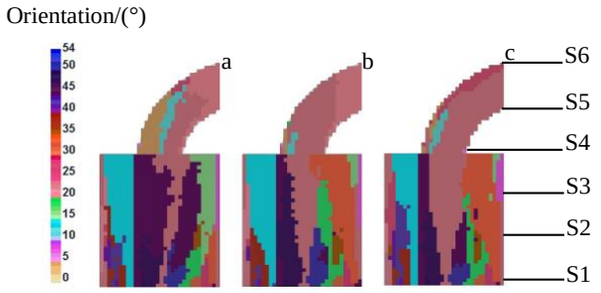

Fig.8 Impact of withdrawal rate on axial distribution of grain growth orientation: (a) 2 mm/min, (b) 5 mm/min, and (c) 8 mm/min

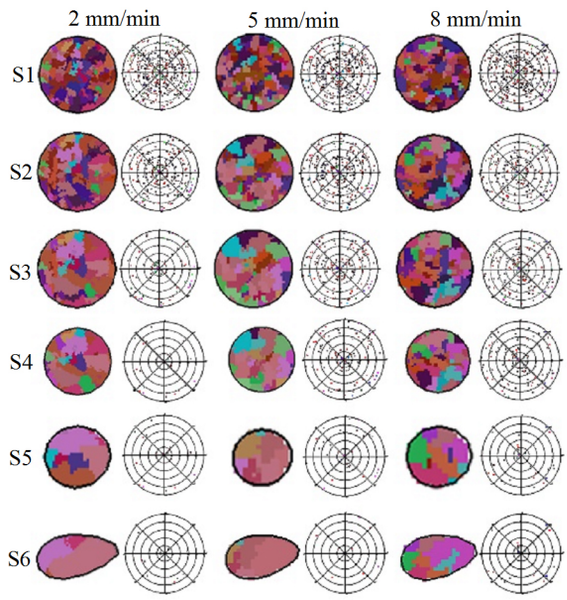

Fig.9 Orientation image maps and corresponding <001> pole figures at different withdrawal rates of different cross sections of spiral selector

selector. As the distance from the chill-plate increases, the secondary arm coarsening occurs in the crystal nuclei close to the <001> orientation of heat flow, which inhibits the grain growth deviating largely from the <001> orientation. The <001> oriented grains occupy the growth space of the solidification microstructure in the crystal selector. Moreover, as shown from the longitudinal direction in Fig.9, the number, area, and color of solidified microstructures at different withdrawal rates in cross section S1 are similar. In cross sections S2 and S3, the number of microstructures at intermediate withdrawal rate is less, the area is larger, and the color is lighter than those at the other two withdrawal rates, which shows that the effect of grain selection with intermediate withdrawal rate is better than that with the other two withdrawal rates.

The orientation image maps and corresponding <001> pole figures of three cross sections (S4~S6) of the spiral part in the spiral selector at withdrawal rates of 2, 5, and 8 mm/min are obtained. In the spiral part of the spiral selector, the solidification structure becomes larger and the color becomes lighter after the evolution of the spiral part, which indicates that the angle between the grain growth direction and <001> orientation becomes smaller. This is because the temperature field and the spatial shape of the selected section play the preliminary roles in grain selection along different directions. As the distance from the chilled plate increases, the nuclei near the direction of the heat flow <001> orientation causes the secondary arm roughening, which inhibits the grain growth with a large deviation from the <001> orientation until the <001> oriented grains occupy the growth space of solidification structure in the crystal selector. Moreover, in cross sections S4 and S5, the number, area, and color of

solidified microstructures at different withdrawal rates are similar. In cross section S6, the number of microstructures with intermediate withdrawal rate is less, the area is larger, and the color is lighter than those with the other two withdrawal rates. It shows that the effect of grain selection with the intermediate withdrawal rate is better at different locations of the crystal selector.

The relationship between the number of grains in the cross sections of the crystal selector and the distance from the chilled surface is shown in Fig.10. With the distance below 4 mm from the chilled surface, the number of grains drops sharply. The reduction rate decreases when the distance from the chilled surface is 4~17 mm. Because there are a large number of nuclei with small microstructures and random grain growth directions on the chilled surface, the competition between grains is fierce at the same undercooling degree, leading to a sharp drop in the number of grains at the initial stage of the starter block of crystal selector. Besides, the growth direction tends to converge. With the distance of 4~17 mm from the chilled surface, the number of grains is small and the growth direction tends to be <001> orientation, and the competition between grains slows down, i.e., the reduction rate of the number of grains reduces. With the distance of 18~35 mm from the chilled surface, the reduction rate decreases and only one kind of grains remains in the end. This is due to the sudden change in the growth space of the remaining grains when they enter the spiral part. The grains with growth direction inconsistent with the direction of the spiral part of crystal selector are eliminated, resulting in a sudden decrease in the number of grains. Therefore, only one kind of grains with <001> orientation remain, thereby achieving the purpose of crystal selection.

The grain selection trend of the spiral selector is the same at different withdrawal rates, but the specific process is different. The number of crystal grains generated on the chilled surface at large and small withdrawal rates is 130, and the number of grains at the intermediate withdrawal rate is 139. The larger number of grains on the chilled surface is beneficial to the selection of grains along the <001> direction. At the end of the starter block (distance from the chilled surface of 17 mm), the number of grains at the intermediate withdrawal rate is smaller than that at small and large withdrawal rates, indicating that the effect of grain selection at intermediate withdrawal rate is better in the starter block. When the <001> oriented grains are selected from the crystal selector at different withdrawal rates, the height at the intermediate withdrawal rate is 32 mm, which is less than that at the small (34 mm) and large (36 mm) withdrawal rates, suggesting that the effect of grain selection at intermediate withdrawal rate is better in the spiral part.

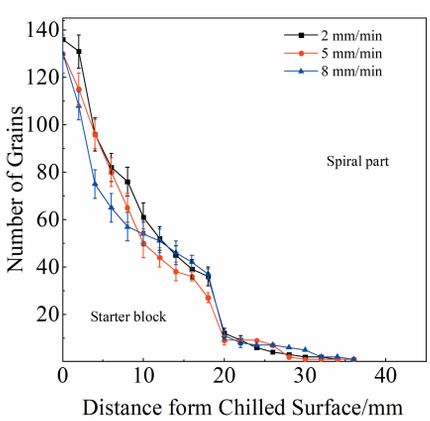

Fig.10 Relationship between the number of grains and distance from the chilled surface

3 Conclusions

1) With increasing the distance from the chilled surface and fixed withdrawal rate, the number of dendrites decreases, and the primary dendrite arm spacing increases gradually. With increasing the withdrawal rate, the primary dendrite arm spacing decreases, the number of dendrite stems increases, and the dendrite structure is refined gradually.

2) The smaller the number of dendrites, the larger the space of dendrite growth, the larger the dendrite spacing, and the faster the selection rate of single crystal. The number of dendrites in the same cross section under the intermediate withdrawal rate (5 mm/min) is less, so the selection efficiency at the intermediate withdrawal rate is better than that at the other two withdrawal rates.

3) During the simulation, the number, area, and color of solid tissues are similar at different withdrawal rates in starter block of spiral selector. In the spiral part, the number of microstructures at intermediate withdrawal rate (5 mm/min) is smaller than that at the other two withdrawal rates, with larger area and lighter color. The results show that in different positions of crystal selector, the effect of middle withdrawal rate is better than that of the other two withdrawal rates.

4) The simulation results are in agreement with experimental results: the grain selection efficiency of the spiral selector at the intermediate withdrawal rate is better than that at the other two withdrawal rates under the same conditions.

References

1 Zhu Xintao, Yang Qiang, Wang Fu *et al. Materials*[J], 2020, 13(5): 1121

2 Zhang Hang, Zhu Xintao, Wang Fu *et al. Materials*[J], 2019, 12(23): 3829

3 Zhu Xintao, Wang Fu, Zhang Shuaipeng *et al. Materials*[J], 2019, 12(11): 1781

4 Li C H, Wei C, Zhang R L *et al. Journal of Central South University*[J], 2018, 25(1): 1

5 Li Yafeng, Liu Lin, Huang Taiwen *et al. Vacuum*[J] 2016, 131: 181

6 Huo Miao, Liu Lin, Yang Wenchao *et al. Vacuum*[J], 2019, 161: 29

7 Yan Xuewei, Zhang Hang, Tang Ning *et al. Progress in Natural*

Science: Materials International[J], 2018, 28(1): 78
8 Zhang Hang, Xu Qingyan. *Materials*[J], 2017, 10(11): 1236
9 Meng Xiangbin, Lu Qi, Li Jinguo *et al. J Mater Sci Technol*[J], 2012, 28(3): 214
10 D'Souza N, Ardakani M G, McLean M *et al. Metall Mater Trans* [J], 2000, 31(11): 2877
11 Zhang Hang, Xu Qingyan, Sun Changbo *et al. Acta Metallurgica Sinica*[J], 2013, 49(12): 1508 (in Chinese)
12 Liu Fencheng, Lin Xin, Yang Gaolin *et al. Rare Met*[J], 2011, 30(1): 433
13 Zheng Qi, Hou Guichen, Tian Weimin *et al. The Chinese Journal of Nonferrous Metals*[J], 2001, 11(2): 176 (in Chinese)
14 Jiang Liwu, Li Shusuo, Han Yafang. *Proc Eng*[J], 2012, 27: 1135 (in Chinese)
15 Yan Xiaofeng, Dong Jianxin, Shi Zhaoxia *et al. Rare Metal Materials and Engineering*[J], 2019, 48(10): 3183 (in Chinese)
16 Esaka H, Shinozuka K, Tamura M. *Mater Sci Eng*[J], 2005, 413: 151
17 Dai H J, Gebelin J C, D'Souza N *et al. Mater Trans*[J], 2009, 22(1-4): 54
18 Zhang Rulin, Chen Lina, Li Chonghe *et al. Trans Nonferrous Met Soc*[J], 2012, 22(5): 1092
19 Zhou Xuefeng, Chen Guang, Feng Yaya *et al. Rare Metal Materials and Engineering*[J], 2017, 46(5): 1245 (in Chinese)
20 Liu Gang, Liu Lin, Ai Cheng *et al*. *J Alloy Compd*[J], 2011, 509 (19): 5866
21 Meng X B, Li J G, Chen Z Q *et al. Metall Mater Trans*[J], 2013, 44(4): 1955
22 Gao Sifeng, Liu Lin, Xu Yiku *et al. China Foundry*[J], 2012, 9(2): 159 (in Chinese)
23 Xu Zilin, Li Zhonglin, Zhang Han *et al. Rare Metal Materials and Engineering*[J], 2017, 46(7): 1856 (in Chinese)
24 Xu Q, Yang C, Zhang H *et al. Metals*[J], 2018, 8(8): 632
25 Wang Yumin, Li Shuangming, Zhong Hong *et al. Acta Metal Sin* [J], 2015, 51(9): 1038 (in Chinese)
26 McCartney D G, Hunt J D. *Acta Metall*[J], 1981, 29(11): 1851
27 Kurz W, Giovanola B, Trivedi R. *Acta Metall*[J], 1986, 34(5): 823
28 Gandin C A, Rappaz M. *Acta Metallurgica et Materialia*[J], 1994, 42(7): 2233
29 Rappaz M, Gandin C A, Desbiolles J L *et al. Metall Mater Trans* [J], 1996, 27(3): 695
30 Xu Qingyan, Liu Baicheng, Pan Dong *et al. China Foundry*[J], 2012, 9(2): 69

抽拉速率对螺旋选晶器选晶行为和晶体取向演变的影响

宗学文[1]，王　磊[1]，刘文杰[1]，张　斌[1]，张凌峰[2]
(1. 西安科技大学 机械工程学院，陕西 西安 710054)
(2. 西安航发精密铸造有限公司，陕西 西安 710021)

摘　要：采用宏观-微观耦合的元胞自动机（CAFE）方法，研究了不同抽拉速率对螺旋选晶器的选晶行为和晶体取向演变的影响，并通过实验对仿真结果进行了验证。结果表明：在相同的抽拉速率下，随着与激冷面距离的增大，枝晶数目逐渐减少，一次枝晶臂间距逐渐增大。随着抽拉速度由2 mm/min增加到8 mm/min，一次枝晶臂间距逐渐减小，枝晶茎数增加，枝晶间距逐渐减小，枝晶组织逐渐细化。在模拟过程中，在螺旋选择器启动块的3种抽拉速率下，固态组织的数量、面积和颜色都是相似的；在螺旋部分，在5 mm/min提取速率下晶体的微结构数量比其他2个提取速率下的少，并且面积更大，颜色更浅。从选晶器的晶粒组织演变和金相组织分析结果可以得出，中等抽拉速率（5 mm/min）下选晶器的选晶效率优于其他2种抽拉速率。

关键词：螺旋选晶器；选晶行为；抽拉速度；定向凝固；一次枝晶间距

作者简介：宗学文，男，1964年生，博士，副教授，西安科技大学机械工程学院，陕西 西安 710054，E-mail：zongw007@xust.edu.cn